Forces in Mechanics 15 (2024) 100273

Contents lists available at ScienceDirect

Forces in Mechanics

journal homepage: www.sciencedirect.com/journal/forces-in-mechanics

Numerical-experimental study on the crashworthiness of a windshield A-pillar

Enrico Armentani [a], Michele Perrella [a,*], Massimiliano Cepollaro [a], Fulvio Cepollaro [b], Giuseppe D'Errico [b], Venanzio Giannella [c]

[a] Department of Chemical, Materials and Production Engineering, University of Naples "Federico II", 80125, Naples, Italy
[b] Stellantis N.V., 80038, Pomigliano D'Arco, NA, Italy
[c] Department of Industrial Engineering, University of Salerno, Fisciano, SA 84084, Italy

ARTICLE INFO

Keywords:
Crashworthiness
Windshield A-pillar
FEM
Impact test
Vehicles

ABSTRACT

This document reports a numerical and experimental crashworthiness study of a vehicle structural component. Particularly, a windshield A-pillar made of a novel high-strength steel was tested on an apparatus for impact tests that was in-house designed so as to reproduce the effects of a vehicle side impact crash. In parallel, numerical simulations were performed using the explicit finite element code LS-DYNA, considering different elastic-plastic material constitutive laws with damage. A comparison between numerical and experimental outcomes demonstrated a satisfactory correlation, with the GISSMO model that provided a good correlation and needed a relatively low computational effort.

1. Introduction

The automotive industry continuously demands for new materials [1,2] and new design concepts in order to satisfy the ever stricter safety requirements. Safety of car occupants is currently achieved by means of preventive, active and passive safety systems [3,4]. Preventive systems can assist the driver while driving, for instance to enhance his vision under adverse conditions [5] or to evaluate his tiredness [6]. The active ones are aimed to reduce the risk of accident occurrence, for example improving stability and control of vehicles [7,8], e.g. by means of anti-lock braking systems (ABS) or electric power steering (EPS). On the contrary, passive systems deal with reducing damages and injuries due to any car fault or crash [9,10].

Amongst these latter, it is worth to mention the crumple zones, devoted to absorbing impact energy during a collision, while the passenger safety cell reacts to vehicle crash and rollover, conveniently deforming itself to best protect occupants. Thus, a suitable design of safety cell components is crucial to reduce passenger injuries [11]. Recent studies have covered investigations on the structural behaviour of innovative materials, such as composites and additively manufactured [12-17], or have investigated new and sustainable manufacturing processes [18–20]. Although these materials have shown optimal strength-to-weight ratio [1,2], their usual high production costs make them unsuitable for large-scale manufacturing. Increasing the know-how regarding new high-strength materials to be used for manufacturing of vehicle structural parts is of fundamental importance to guarantee competitive advantages in the automotive market. Besides, this also enables the possibility to improve the response of the vehicle in terms of safety and resistance, thus obtaining better results in crash-tests [12]. At the same time, there is also the possibility of enhancing the performance of a car and increasing the quality perceived by users thanks to the advantages in terms of mass reduction provided by new technologies.

Safety of a car roof in rollover crashes is favoured by high-strength A-pillars. When using traditional metal materials for A-pillars, their design inherently requires size increments that can affect the lateral view of the driver, producing blind spots when turning [21]. Indeed, these are elements that need an appropriate sizing in order to guarantee both a satisfactory clean lateral view and a harmless safety cell. The use of high-strength steels allows to produce A-pillars of reduced dimensions but keeping the same strength offered by traditional materials.

Within this framework, this research aimed to assess the impact behaviour of a windshield A-pillar, a constituent part of the safety cell of a modern vehicle. An impact test apparatus was ad-hoc designed by the Authors in order to experimentally investigate the crash behaviour of an A-pillar made of a novel high-strength steel. In parallel, numerical

* Corresponding author.
E-mail address: michele.perrella@unina.it (M. Perrella).

https://doi.org/10.1016/j.finmec.2024.100273
Received 26 March 2024; Received in revised form 9 May 2024; Accepted 10 May 2024
Available online 14 May 2024

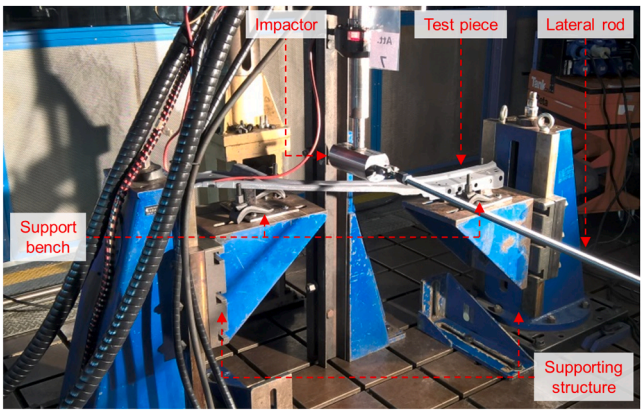

Fig. 1. Ad-hoc designed impact test apparatus.

modelling was used to support the experiments so as to achieve a better comprehension of test results and also for acquiring a deeper comprehension on the mechanisms of failure. Therefore, numerical analyses were performed by means of the explicit finite element code LS-DYNA so as to cross-compare results with those obtained experimentally. Such a numerical-experimental cross-validation can be considered a common practice in the modern engineering field, as it is often used to develop safer and "greener" vehicles, in addition to the advantage of reducing costs required by full-scale experiments [22–27].

2. Test apparatus

An experimental testing apparatus was in-house designed to acquire the response of a windshield A-pillar subjected to impact loading, see Fig. 1. The design of the test was orientated to replicate as reliably as possible the effects that occur on this element during a lateral impact while driving. This was of particular interest for what concerning the proper location and orientation of the test piece.

The experimental device consists of a hydraulic actuator for the load application, a supporting system and a data acquisition system. The actuator is equipped with a cylindrical threaded impactor that is connected to a longitudinal rod, this latter required in order to prevent unwanted oscillations transversal to the impact direction. A load cell of 100 kN was used to measure the crash force during the test (see centre top of Fig. 1). A linear variable displacement transducer, located at the bottom of the actuator, was used to measure the displacement along the test. The supporting system is adjustable in height since the A-pillar is not planar and the span can be set according to the dimensions of the test piece. Once defined the test span, two ad-hoc bench supports are welded to the A-pillar sample, in the same points where it would be fixed to the load-bearing structure of the vehicle, i.e. to achieve the most realistic constraint conditions. The support benches are in turn bolted to the supporting structure. The so obtained test apparatus is highly modular and allows to verify the impact behaviour of components with different sizes and shapes.

Table 1
Mechanical properties of the selected HSLA steel.

Mass density ρ [kg/m^3]	Young's modulus E [GPa]	Poisson' ratio ν [–]
7850	208	0.32

The cylindrical impactor is made of steel and presents a cross section diameter of 100 mm and a length of 200 mm. Two different loading conditions can be applied: free-fall drop impact and displacement-controlled loading. The latter boundary condition was adopted for the experiments reported herein. The impact rates that can be imposed to the actuator range from 0.1 to 2.5 m/s. A trapezoidal motion profile with an acceleration, constant speed and deceleration was imposed. The actuator displacement was opportunely set so as to neglect unwanted inertia effects and was properly calibrated in order to achieve the crash when the impactor already reached the constant speed condition. The current test was carried out under constant impact speed applying to the impactor a displacement of 180 mm at 180 ms. Test parameters were selected within the technological performances of the testing machine and defined so as to emulate the behaviour of the component in a full-scale vehicle side impact.

The support benches were made of welded S235 steel sheets with different thicknesses (5 and 10 mm) so as to satisfy specific requirements in terms of overall stiffness. As a matter of fact, the two support benches have to be stiff enough to ensure breakage of the windshield spar, whereas a high deformable support could bend excessively during impact, in turn reducing the actual stresses to which the A-pillar is subjected. Besides, excessively stiff supports could cause the unwanted cutting of welded zones between support benches and the test piece before the onset of fracture in the area of impact.

3. Materials and methods

The impact test was performed on a windshield A-pillar sample, see Fig. 2. This component was manufactured through hot stamping starting from a 1.2-mm thick foil of a high-strength low alloy (HSLA) steel. The main mechanical properties of the selected HSLA steel make it particularly suitable for the realization of vehicle structural components by hot stamping technology (some properties were listed in Table 1). Such a

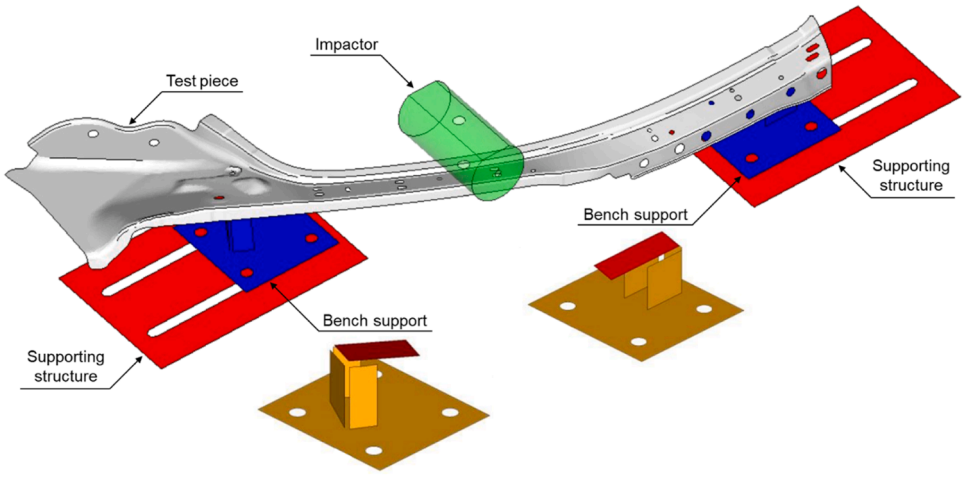

Fig. 2. CAD model of the impact test on the windshield A-pillar.

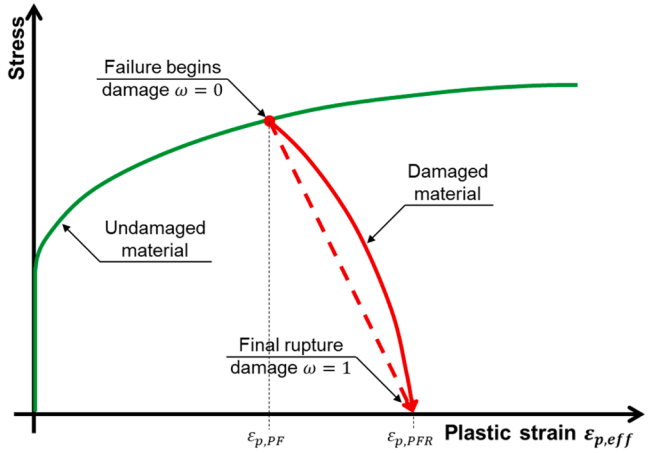

Fig. 3. Stress vs. effective plastic strain with damage effects (MAT_081).

material is currently protected by industrial secrecy of Stellantis. Experimental results were reported in terms of crushing load-displacement curves and energy absorption (EA) during impact, which are considered as particularly representative crashworthiness indicators [28,29]. The absorbed energy was obtained as it follows:

$$EA = \int_0^d P(s)ds, \tag{1}$$

where $P(s)$ is the crash force during the test, d is the displacement at breaking point, s is the displacement.

Numerical analyses based on Finite Element Method (FEM) were carried out to replicate the impact test in a simulation environment. To this aim, a CAD model was set up as shown in Fig. 2. Based on this CAD model, FEM analyses were developed by means of the commercial FEM code LS-DYNA [30]. Particularly, two material models were adopted:

1. an elastic-plastic law with damage and embedded failure criterion (so called "MAT_081" in the FEM code manual [30]),
2. the generalized incremental stress state dependaent damage model (GISSMO) [30,31].

Briefly, with model (1), a user-defined stress-strain curve is defined to simulate the elastic-plastic behaviour of the material under analysis. The effective stress is considered as a function of the effective plastic strain, this latter depending on the strain rate. A failure criterion is activated once an imposed plastic strain $\varepsilon_{p,PF}$ is reached. An isotropic damage parameter ω is evaluated as it follows:

$$\omega = \frac{\varepsilon_{p,eff} - \varepsilon_{p,PF}}{\varepsilon_{p,PFR} - \varepsilon_{p,eff}}, \tag{2}$$

where $\varepsilon_{p,eff}$ is the effective plastic strain, $\varepsilon_{p,PF}$ is the plastic strain value in correspondence of softening onset, $\varepsilon_{p,PFR}$ is the plastic strain to final rupture (see Fig. 3). The amount of the linear cumulative damage ω ranges from zero to one, representing no damage and complete failure respectively.

With reference to model (2), GISSMO model was developed as an extension of the Johnson-Cook failure criterion to overcome the differences in simulation results between metal forming and crash tests [32]. GISSMO is based on a phenomenological approach that estimates an incremental damage or, more properly, a phenomenological scalar failure variable coupled with the deformation process. Hence, it is completely general and allows for the modelling of a failure phenomenon for any type of simulation.

The GISSMO damage parameter is evaluated by means of an incremental law obtained from empirical observations. The damage accumulation can be defined as:

$$D = \left(\frac{\varepsilon_p}{\varepsilon_f(\eta,\ \theta)}\right)^n, \tag{3}$$

where ε_p is the equivalent plastic strain, n is an exponent for the damage function, $\varepsilon_f(\eta,\ \theta)$ is the equivalent plastic fracture strain that depends on the triaxiality parameter η and Lode angle θ.

For the Johnson-Cook failure criterion, the exponent n is equal to 1. The triaxiality parameter η is defined as the ratio between the hydrostatic stress σ_m and the von Mises equivalent stress σ_{eq}. The Lode angle θ is related to the second and third deviatoric stress tensors, J_2 and J_3, as it follows:

$$\theta = \frac{1}{3}\arccos\left(\frac{3\sqrt{3}\,J_3}{2\,J_2^{\frac{3}{2}}}\right) \tag{4}$$

Considering the Haigh-Westergaard domain, the stress state is uniquely defined by knowing the quantities σ_{eq}, η and θ. By derivation of Eq. (3), under the hypothesis of constant ε_f, i.e. proportional loading, the incremental damage is:

$$dD = \frac{n}{\varepsilon_f^n(\eta,\ \theta)}\,\varepsilon_p^{(n-1)}\,d\varepsilon_p = f\left(\varepsilon_f(\eta,\ \theta),\ \varepsilon_p,\ n\right)d\varepsilon_p, \tag{5}$$

where f is function of $\varepsilon_f(\eta,\ \theta)$, ε_p and n.

By substituting Eq. (3) in Eq. (5), the GISSMO incremental damage relationship is:

$$dD = \frac{n}{\varepsilon_f(\eta,\ \theta)}\,D^{\frac{n-1}{n}}\,d\varepsilon_p = f\left(\varepsilon_f(\eta,\ \theta),\ D,\ n\right)d\varepsilon_p, \tag{6}$$

where D is the current damage and f is directly function of D instead of accumulated plastic strain.

The local material instabilities, such as necking phenomenon, are considered by means of an additional variable, called potential instability F that is expressed as

$$F = \left(\frac{\varepsilon_p}{\varepsilon_{crit}(\eta)}\right)^n, \tag{7}$$

where $\varepsilon_{crit}(\eta)$ is the critical plastic strain that is function of η. This variable is experimentally evaluated by using curves from tensile tests and depends on the material forming limit diagram curve. The experimental procedure for these evaluations is described in [33].

By differentiation of Eq. (6) under the assumption of constant η:

$$dF = \frac{n}{\varepsilon_{crit}(\eta)}\,F^{\frac{n-1}{n}}\,d\varepsilon_p = f\left(\varepsilon_{crit}(\eta),\ F,\ \varepsilon_p\right)d\varepsilon_p, \tag{8}$$

where F is the value of the current instability.

The evaluation of damage and instability variables allows for assessing the stress field degradation. Defined σ^* the effective stress tensor and σ the undamaged stress tensor, it follows:

$$\sigma^* = \begin{cases} \sigma & D \le D_c \\ \sigma\left[1 - \left(\dfrac{D - D_c}{1 - D_c}\right)^m\right] & D \ge D_c \end{cases}, \tag{9}$$

where the fading exponent m triggers the stress degradation of element, whereas D_c is the critical damage when instability is equal to 1.

4. FEM analysis

Numerical simulations were performed with the LS-DYNA code, using Hypermesh [34] as pre-processors and Hyperview as post-processor. Shell elements were used for the FEM discretization of the CAD model, selecting fully integrated elements and five through-the-thickness integration points (so called ELFORM 16 in the

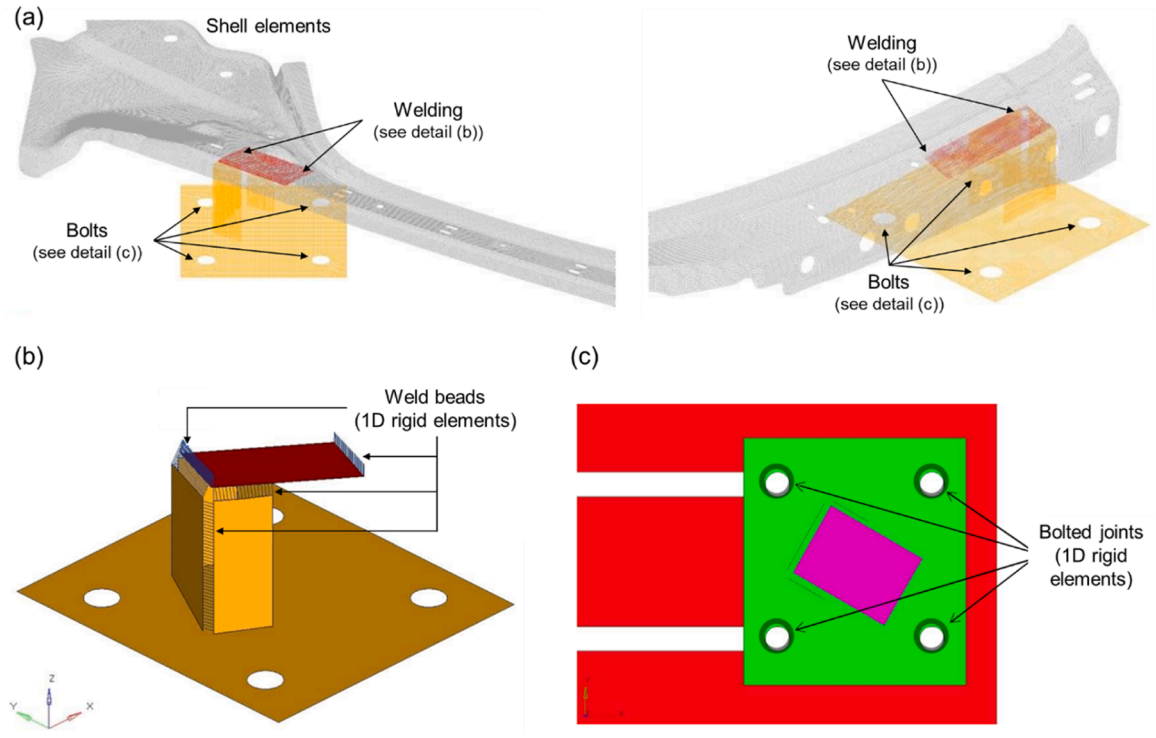

Fig. 4. (a) FEM model of the impact test on the windshield A-pillar; (b-c) close-up views of the supporting structure modelling.

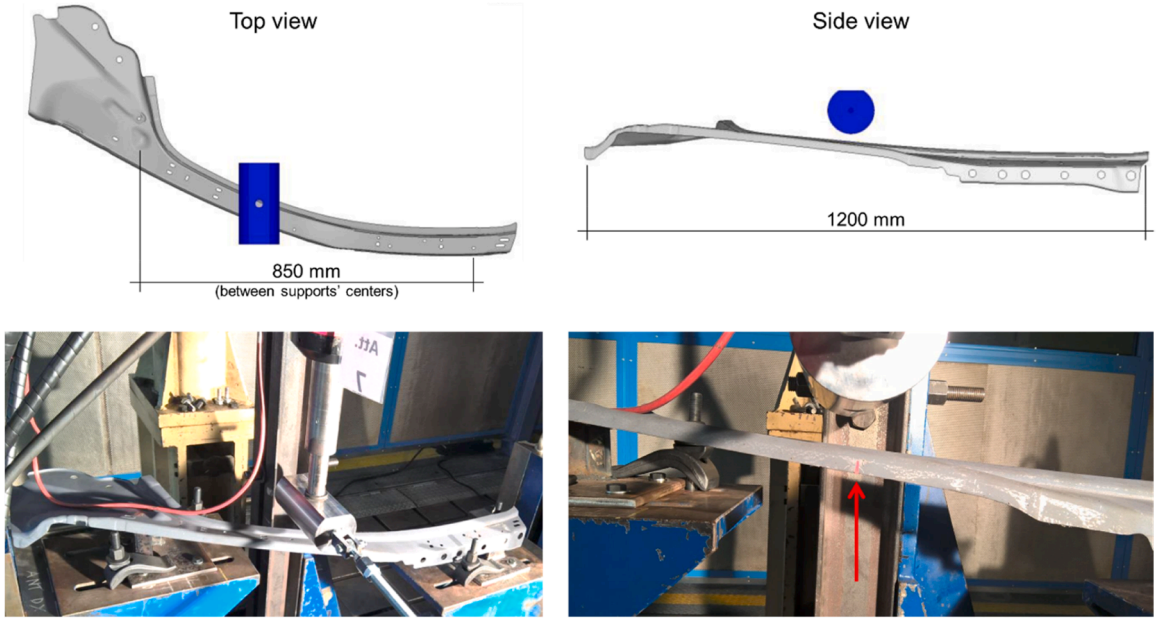

Fig. 5. Initial position of the impactor with respect to the windshield A-pillar.

FEM code library). The average mesh size was around 2 mm to accurately capture the onset of failure and the damage propagation mechanisms. The convergence study was developed by comparing the hourglass energy and added mass for various model of increasing computational burden. Such convergence was judged as achieved when added mass and hourglass energy were lower than 1% of the component mass and internal energy respectively. For the sake of brevity, only the results developed with the best model were reported herein. Fig. 4a shows the resulting FEM model. The impactor was modelled as rigid with respect to the A-pillar sample, hence allowing to reduce the overall computation burden. Constraints were applied to the impactor to allow for vertical displacements only.

Particular attention was devoted to the discretization of the bench supporting structure, see Figs. 4b-c. The weld beads were modelled by means of rigid 1D elements coupling the nodes of the parts in such a way to model their weldments. This allowed to model 1D elements parallel to each other, which prevented any relative sliding between the components, thus accurately simulating the weld bead behaviour. The so obtained FEM model resulted in a particularly accurate mesh of the A-pillar, having a perfect correspondence amongst the relative nodes and those belonging to the supporting elements. Besides, bolted joints of the supporting system were modelled using the LS-DYNA card

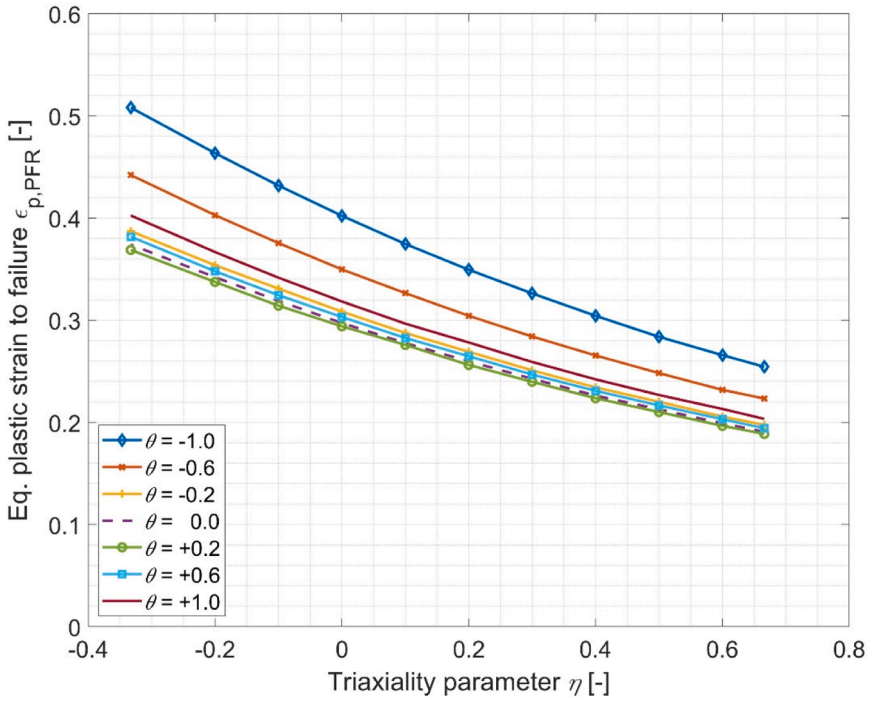

Fig. 6. Equivalent plastic strain to failure vs. triaxiality parameter as a function of Lode angle θ.

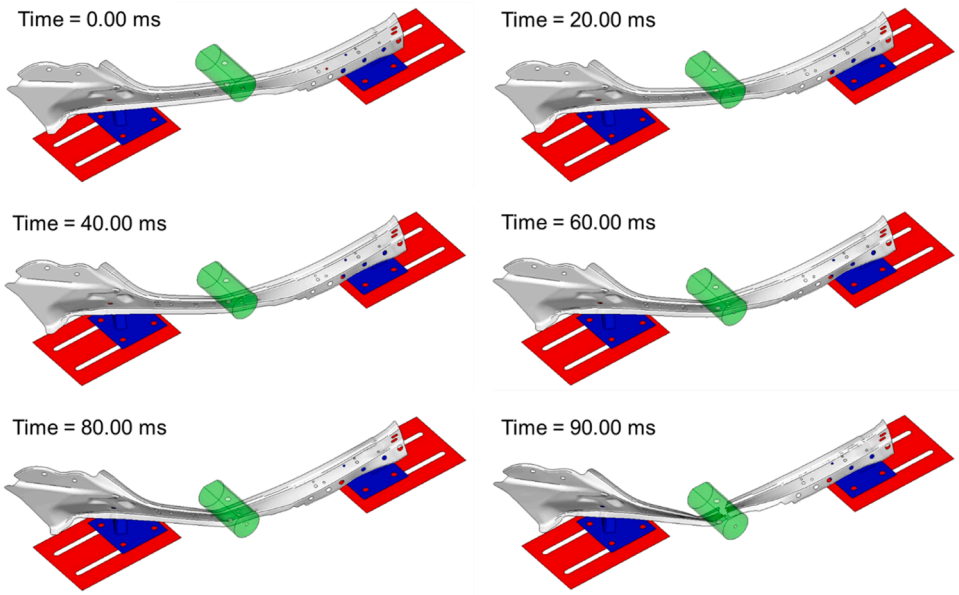

Fig. 7. Impact test simulation at some time frames.

*CONSTRAINED_EXTRA_NODES, which allowed to rigidly connect the two parts. Specifically, the nodes in correspondence of the holes belonging to each support (see Fig. 4c) were rigidly constrained to the respective support system base.

Hourglass effect was controlled by setting the ELFORM parameter equal to 16. Any element was removed by the simulation when one of its integration points reached the failure condition of the selected criterion. The automatic contact algorithm was used for the tied surfaces of the cylindrical impactor and the A-pillar. Initial position of the impactor was highlighted in Fig. 5. As reported in above, the experimental test was not performed as a free-fall drop impact but as a displacement-controlled loading. Hence a trapezoidal motion profile with acceleration, regime and deceleration was applied to the actuator. This same motion profile was also considered numerically.

Referring to the analyses implementing the MAT_081 material model, the logarithmic values of $\varepsilon_{p,PF}$ and $\varepsilon_{p,PFR}$ for the first attempt simulation (herein Run 01) were set to 0.1 and 0.15, respectively. Additionally, due to lack of dedicated data, two further calculations (Run 02–03) were made by considering the plastic strain at final rupture $\varepsilon_{p,PFR}$ equal to 0.3 and 0.5 respectively. Accordingly, FEM simulations with the GISSMO model were performed by varying the parameter SFO. This parameter allows to proportionally modify the equivalent plastic strain to failure vs. triaxiality curves, thus changing the material softening phase and consequently the time to rupture. These curves, plotted in Fig. 6 and identified in the LS-DYNA code by the variable LCSDG, are

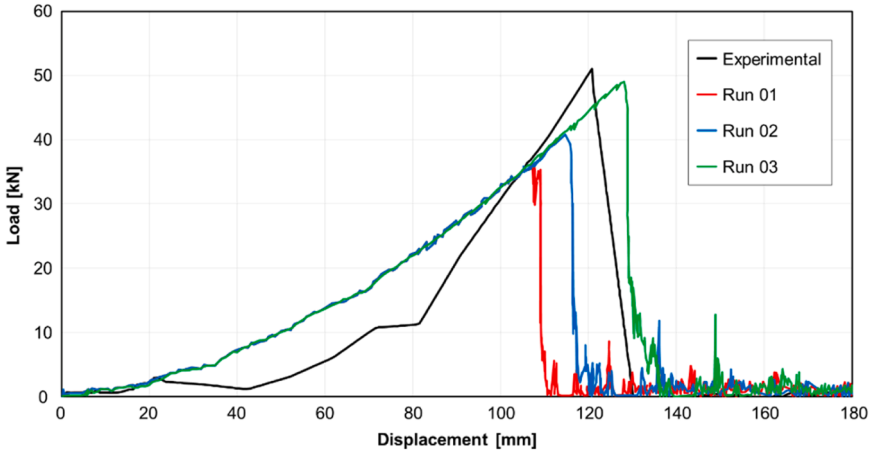

Fig. 8. Comparison of experimental and numerical load-displacement curves (MAT_081).

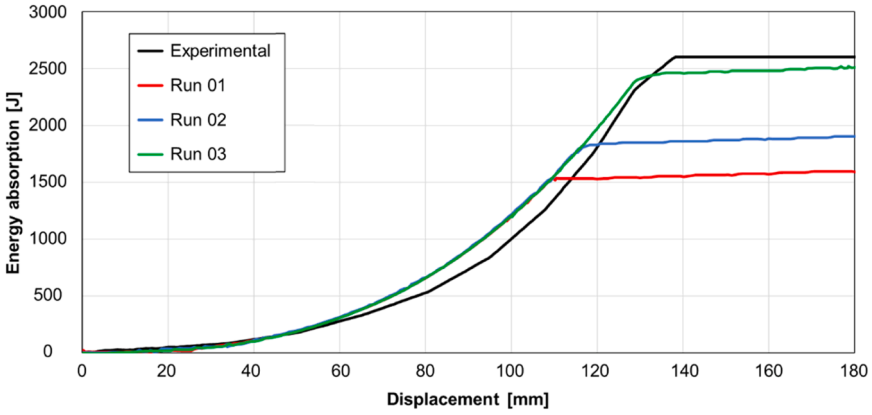

Fig. 9. Trend of impact energy as function of displacement (MAT_081).

functions of the Lode angle θ, ranging from −1 to 1. The value of SFO for the first attempt analysis (Run 04) was set to 1 and two further calculations (Run 05-06) were made by considering SFO equal to 1.1 and 1.5 respectively.

5. Results and discussion

Numerical analyses were conducted by applying MAT_081 and GISSMO material models in order to replicate the impact test. An example sequence of the simulated crash test was shown in Fig. 7. The comparison of results coming from the experimental tests and the FEM modelling considering the MAT_081 were reported in Figs. 8 and 9 (Run 01-03). Such figures highlight a reasonable agreement in terms of load and energy absorption over the impactor's displacement, even though simulation outcomes demonstrate a ductile behaviour not represented by the experimental response. Indeed, when the test starts, the impactor touches only partially the whole width of the test piece, hence finding a variable stiffness of the piece during the impact. This can be also noticed

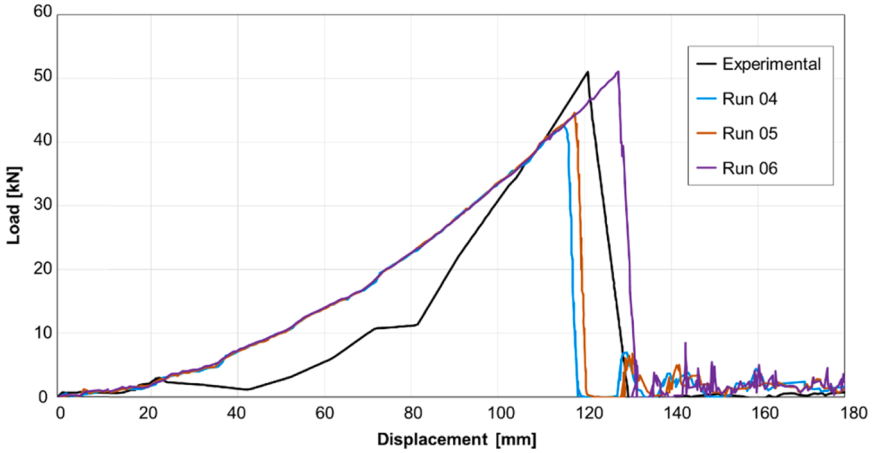

Fig. 10. Comparison of experimental and numerical load-displacement curves (GISSMO).

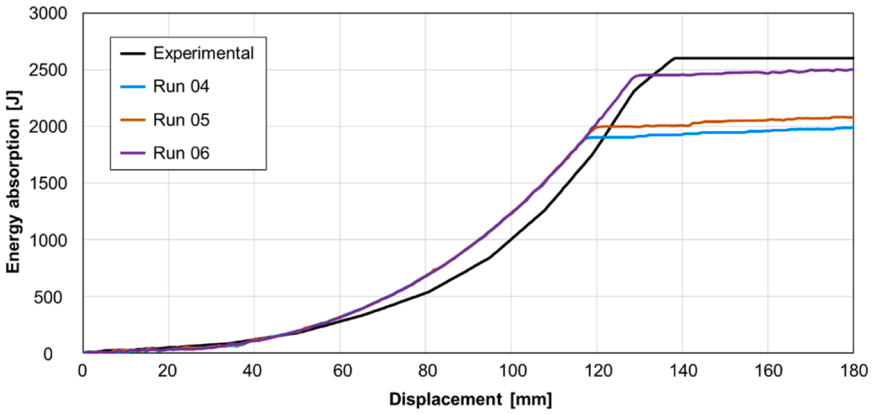

Fig. 11. Trend of impact energy as function of displacement (GISSMO).

Table 2
Main outcomes of all impact simulations.

	SFO [-]	$\varepsilon_{p,PFR}$ [-]	Peak load [kN]	Displacement at break [mm]	Absorbed energy [J]
Experiment	–	–	51	120	2605
Run 01	–	0.15	37	106	1614
Run 02	–	0.3	41	117	1800
Run 03	–	0.5	49	128	2531
Run 04	1	–	42	116	2020
Run 05	1.1	–	43	118	2040
Run 06	1.5	–	51	128	2540

by looking at the right side of Fig. 5, where it is visible a slight initial torsion of the test piece caused by its welding on the bench supports. Since this initial deformation was not simulated numerically, a slightly different stiffness can be observed between numerical and experimental outcomes. As a consequence, the lower energy absorption calculated numerically represents a result of the calculated displacements at break and maximum loads lower than those measured experimentally. The calibration of numerical failure effect was realized by increasing the plastic strain at final rupture $\varepsilon_{p,PFR}$ until that the percentage difference in the maximum force less than 4% was reached (Run 03). The resulting crash energy was 3% lower than that experimentally recorded, although the model predicted its achievement in a slightly different time lapse. This discrepancy was ascribed to a more compliant behaviour of bench supports.

The trends of load and impact energy vs. displacement with reference to the GISSMO material model were plotted in Figs. 10 and 11. According to the MAT_081 simulations, a convergence to experimental results was performed by varying the SFO parameter from 1 to 1.5. It can be noticed in Figs. 10 and 11 that the best agreement was achieved by setting the SFO parameter to 1.5.

The main outcomes of all the impact simulations were summarised in Table 2 and Fig. 12 as percentage differences amongst the two models for F_{max}, U_{max} and AE. An overall good correlation with experimental outcomes can be noticed for both material models. Moreover, it is worth noting that GISSMO simulations resulted in a higher accuracy than MAT_081 to not count the fact that also required lower calculation times. Once achieved such a correlation, this simulation procedure can be replicated by considering different geometries and materials, hence supporting the design and/or the optimization of passive safety systems, in turn improving the vehicle crashworthiness.

6. Conclusions

The optimum design of passenger safety cells of modern vehicles is crucial to reduce occupants' injuries due to any car fault or accident. This document reports a numerical-experimental crashworthiness analysis of a windshield A-pillar, a fundamental component for the passive safety of vehicles. An experimental testing apparatus was in-house designed in order to replicate as reliably as possible the effects

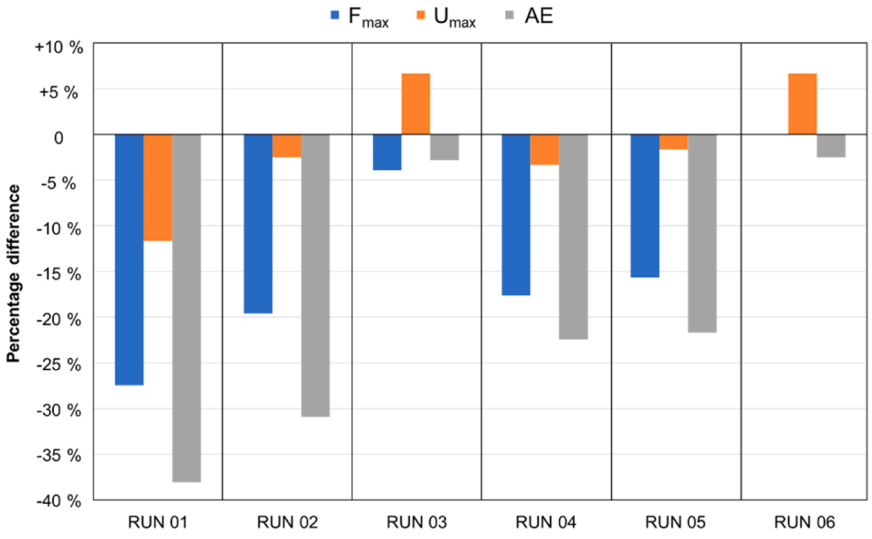

Fig. 12. Overall comparison of FEM results to experimental outcomes.

that occur on an A-pillar during a lateral impact while driving. Separately, numerical simulations were performed using the explicit FEM code LS-DYNA, considering different material models with damage so as to reach a better explanation of the impact phenomenon. The agreement between numerical and experimental results can be considered as satisfactory. In more details, the GISSMO model resulted to be more suitable than MAT_081 demonstrating a both better prediction of the impact behaviour and also requiring a lower computational effort. Nonetheless, it is worth noting that both models can achieve good correlation with experiments in terms of maximum impact force, maximum displacement, and absorbed energy. This investigation can be useful for improving the crashworthiness of vehicles, providing information to support design and optimization of passive automotive safety systems.

CRediT authorship contribution statement

Enrico Armentani: Writing – original draft, Visualization, Supervision, Conceptualization. **Michele Perrella:** Writing – original draft, Visualization, Data curation. **Massimiliano Cepollaro:** Software, Investigation, Formal analysis, Data curation. **Fulvio Cepollaro:** Validation, Supervision, Software, Resources, Conceptualization. **Giuseppe D'Errico:** Writing – original draft, Supervision, Methodology, Conceptualization. **Venanzio Giannella:** Writing – review & editing, Writing – original draft, Visualization, Validation, Data curation.

Declaration of competing interest

The authors declare that they have no known competing financial interests or personal relationships that could have appeared to influence the work reported in this paper.

Data availability

The data that has been used is confidential.

References

[1] R. Sepe, V. Giannella, N. Razavi, F. Berto, Characterization of static, fatigue and fracture behaviour of the aluminium-lithium alloy Al-Li 2198-T851, Int. J. Fatigue 166 (2023) 107265, https://doi.org/10.1016/j.ijfatigue.2022.107265.

[2] R. Sepe, V. Giannella, P. Mazza, E. Armentani, S.M. Javad Razavi, F. Berto, Fatigue fracture tests on Al-Li 2198-t851 specimens under mixed-mode conditions, in: Proceedings of the Procedia Structural Integrity 39, Elsevier, Amsterdam, the Netherlands, 2021, pp. 546–551, https://doi.org/10.1016/j.prostr.2022.03.127.

[3] P. Du Bois, C.C. Chou, B.B. Fileta, T.B. Khalil, A.I. King, H.F. Mahmood, H.J. Mertz, J. Wismans, Vehicle crashworthiness and occupant protection, in: Priya Prasad, Jamel E. Belwafa (Eds.), Automotive Applications Committee, American Iron and Steel Institute, Southfield, Michigan, USA, 2004.

[4] J.A.C. Ambrosio, Design and calculation of energy absorbing systems, in: J.A. C. Ambrosio (Ed.), Crashworthiness. International Centre For Mechanical Sciences (Courses and Lectures), Springer, Vienna, 2001, https://doi.org/10.1007/978-3-7091-2572-4_10 vol 423.

[5] J.F. González-Saavedra, M. Figueroa, S. Céspedes, S. Montejo-Sánchez, Survey of cooperative advanced driver assistance systems: from a holistic and systemic vision, Sensors 22 (2022) 3040.

[6] Rui Li, Yingjie Victor Chen, Linghao Zhang, A method for fatigue detection based on Driver's steering wheel grip, Int. J. Ind. Ergon. 82 (2021) 103083.

[7] T. Fiorentin, T. De Borba, Comparison Of Performance In Vehicle Braking With Active And Inactive ABS System, SAE Technical Paper, 2022, 2021-36-0072.

[8] S. Na, Z. Li, F. Qiu, C. Zhang, Torque control of electric power steering systems based on improved active disturbance rejection control, Math. Probl. Eng. 6509607 (2020) 2020.

[9] N.A.Z. Abdullah, M.S.M. Sani, M.S. Salwani, N.A. Husain, A review on crashworthiness studies of crash box structure, Thin-Walled Struct. 153 (2020) 106795.

[10] P. Jongpradist, N. Saingam, P. Tangthamsathit, P. Chanpaibool, J. Sirichantra, S. Aimmanee, Crashworthiness analysis and design of a sandwich composite electric bus structure under full frontal impact, Heliyon 8 (12) (2022) e11999, https://doi.org/10.1016/j.heliyon.2022.e11999, 5.

[11] P. King, Accidental injury, biomechanics and prevention, IEEE Eng. Med. Biol. Mag. 21 (2002) 107.

[12] A. Borrelli, G. D'Errico, C. Borrelli, R. Citarella, Assessment of crash performance of an automotive component made through additive manufacturing, Appl. Sci. 10 (2020) 9106, https://doi.org/10.3390/app10249106.

[13] T. Anderson, E. Madenci, Experimental investigation of low-velocity impact characteristics of sandwich composites, Compos. Struct. 50 (2000) 239–247.

[14] E. Armentani, I. Del Prete, R. Sepe, C. Borrelli, G. D'Errico, Optimization of an absorber for improving performances in a leg impact, in: In Proceedings of the 45°AIAS National Conference, Trieste, Italy, 7-10 September, 2016.

[15] A. Masoumi, M.H. Shojaeefard, A. Najibi, Comparison of steel, aluminum and composite bonnet in terms of pedestrian head impact, Saf. Sci. 49 (2011) 1371–1380.

[16] M. Abdullah, W. Cantwell, The impact resistance of polypropylene-based fibre–metal laminates, Compos. Sci. Technol. 66 (2006) 1682–1693.

[17] A. Sellitto, A. Riccio, G. Magno, G. D'Errico, G. Monsurrò, A. Cozzolino, Feasibility study on the redesign of a metallic car hood using composite materials, Int. J. Automot. Technol. 21 (2020) 471–479.

[18] A. Astarita, A. Squillace, E. Armentani, S. Ciliberto, Friction stir welding of AA 2198 T3 rolled sheets in butt configuration, Metall. Italiana 104 (2012) 31–40. ISSN: 0026-0843.

[19] F. Bollino, V. Giannella, E. Armentani, R. Sepe, Mechanical behavior of chemically-treated hemp fibers reinforced composites subjected to moisture absorption, J. Mater. Res. Technol. 22 (2023) 762–775, https://doi.org/10.1016/j.jmrt.2022.11.152.

[20] R. Citarella, V. Giannella, Additive Manufacturing in Industry, Appl. Sci. 11 (2021) 840, https://doi.org/10.3390/app11020840.

[21] M. Sivak, B. Schoettle, M.P. Reed, M.J. Flannagan, Body-pillar vision obstructions and lane-change crashes, J. Saf. Res. 38 (5) (2007) 557–561, https://doi.org/10.1016/j.jsr.2007.06.003.

[22] F. Caputo, A. De Luca, A. Greco, A. Marro, A. Apicella, R. Sepe, E. Armentani, Established numerical techniques for the structural analysis of a regional aircraft landing gear, Adv. Mater. Sci. Eng. 2018 (2018) 536581, https://doi.org/10.1155/2018/8536581.

[23] F. Caputo, G. Lamanna, D. Perfetto, A. Chiariello, F. Di Caprio, L. Di Palma, Experimental and numerical crashworthiness study of a full-scale composite fuselage section, AIAA J. 59 (2) (2021) 700–718.

[24] W. Gao, G. Zhao, X. He, S. Chen, C. Wang, A high-fidelity numerical approach for dummy head-windshield contact interactions, Int. J. Impact Eng. 176 (2023) 104560, https://doi.org/10.1016/j.ijimpeng.2023.104560.

[25] M. Guida, G. Lamanna, F. Marulo, F. Caputo, Review on the design of an aircraft crashworthy passenger seat, Progr. Aerosp. Sci. 129 (2022) 100785, https://doi.org/10.1016/j.paerosci.2021.100785.

[26] E. Armentani, F. Caputo, L. Esposito, V. Giannella, R. Citarella, Multibody simulation for the vibration analysis of a turbocharged diesel engine, Appl. Sci. 8 (2018) 1192, https://doi.org/10.3390/app8071192.

[27] V. Giannella, C. Colangeli, J. Cuenca, R. Citarella, M. Barbarino, Experimental/numerical acoustic assessment of aircraft seat headrests based on electrospun mats, Appl. Sci. 11 (2021) 6400, https://doi.org/10.3390/app11146400.

[28] L. Di Palma, F. Di Caprio, A. Chiariello, M. Ignarra, S. Russo, A. Riccio, A. De Luca, F. Caputo, Vertical drop test of composite fuselage section of a regional aircraft, AIAA J. 58 (1) (2020) 474–487, https://doi.org/10.2514/1.J058517.

[29] F. Di Napoli, A. De Luca, F. Caputo, F. Marulo, M. Guida, B. Vitolo, Mixed FE–MB methodology for the evaluation of passive safety performances of aeronautical seats, Int. J. Crashworth. 24 (3) (2019) 314–325, https://doi.org/10.1080/13588265.2018.1441616.

[30] Livermore Software Technology Corporation (LSTC), LS-DYNA Keyword User's Manual, Version 971 R6.1.0, Vol. 1 and 2, 2012.

[31] F. Neukamm, M. Feucht, A. Haufe, Considering damage history in crashworthiness simulations, in: Proceedings of the 7th European LS-DYNA Conference, Salzburg, Austria, 2009.

[32] G.R. Johnson, W.H. Cook, Fracture characteristics of three metals subjected to various strains, strain rates, temperatures and pressures, Eng. Fract. Mech. 21 (1985) 31–48.

[33] ISO 12004-2, Metallic Materials - Determination of Forming-Limit Curves For Sheet and Strip - Part 2: Determination of Forming-Limit Curves in the Laboratory, 2021.

[34] Altair Engineering, Hypermesh User Manual, Altair Engineering, Troy, MI, USA, 2011.